Coupling a sensory hair-cell bundle to cyber clones enhances nonlinear amplification

Jérémie Barral[a,1], Kai Dierkes[b,1], Benjamin Lindner[b], Frank Jülicher[b], and Pascal Martin[a,2]

[a]Laboratoire Physico-Chimie Curie, Centre National de la Recherche Scientifique, Institut Curie, Université Pierre et Marie Curie, 75005 Paris, France; and [b]Max Planck Institute for the Physics of Complex Systems, 01187 Dresden, Germany.

Edited by A. J. Hudspeth, Howard Hughes Medical Institute, New York, NY, and approved March 5, 2010 (received for review November 26, 2009)

The vertebrate ear benefits from nonlinear mechanical amplification to operate over a vast range of sound intensities. The amplificatory process is thought to emerge from active force production by sensory hair cells. The mechano-sensory hair bundle that protrudes from the apical surface of each hair cell can oscillate spontaneously and function as a frequency-selective, nonlinear amplifier. Intrinsic fluctuations, however, jostle the response of a single hair bundle to weak stimuli and seriously limit amplification. Most hair bundles are mechanically coupled by overlying gelatinous structures. Here, we assayed the effects of mechanical coupling on the hair-bundle amplifier by combining dynamic force clamp of a hair bundle from the bullfrog's saccule with real-time stochastic simulations of hair-bundle mechanics. This setup couples the hair bundle to two virtual hair bundles, called cyber clones, and mimics a situation in which the hair bundle is elastically linked to two neighbors with similar characteristics. We found that coupling increased the coherence of spontaneous hair-bundle oscillations. By effectively reducing noise, the synergic interplay between the hair bundle and its cyber clones also enhanced amplification of sinusoidal stimuli. All observed effects of coupling were in quantitative agreement with simulations. We argue that the auditory amplifier relies on hair-bundle cooperation to overcome intrinsic noise limitations and achieve high sensitivity and sharp frequency selectivity.

auditory amplifier | hair-bundle motility | coupled oscillators | fluctuations

The vertebrate ear is mechanically active. By producing mechanical work to boost vibrations of its sensory organs, the ear enhances its sensitivity and sharpens its frequency selectivity to faint stimuli (1–4). Current theoretical descriptions of this active process are based on oscillator modules (3, 5). Despite viscous friction, each module can be turned into a highly tuned resonator if active feedback generates negative damping (6). Above a critical value of feedback gain, the system oscillates spontaneously. Near an oscillatory instability, any active dynamical system is ideally suited to detect periodic stimuli, for it acts as a frequency-selective, nonlinear amplifier (5, 7–10).

Hair cells, the sensory receptors in the inner ear, can power active mechanical movements of their mechano-sensitive hair bundle, including spontaneous oscillations (11–16). Although active hair-bundle motility provides a plausible component of the active process in vivo, amplification at the scale of a single hair bundle (10) is much less effective than the active process in an intact organ (17). Intrinsic fluctuations destroy the phase coherence of hair-bundle oscillations and limit the gain of the hair-bundle amplifier (18–20). In vivo, hair bundles are generally mechanically coupled by an overlying gelatinous matrix. Thus, active oscillator modules might each recruit a group of coupled hair bundles. It was proposed on theoretical grounds that coupled hair bundles may cooperate to improve their performance (21).

Here we developed a dynamic force-clamp procedure to assay experimentally the effects of mechanical coupling on the hair-bundle amplifier. We emulated elastic coupling to two flanking neighbors by interfacing micromanipulation of a single hair bundle with real-time computer simulations of virtual cells called "cyber clones." We measured the effects of coupling on spontaneous hair-bundle oscillations and on amplification of sinusoidal stimuli. We show that a hair bundle connected to noisy oscillators with similar characteristics outperforms one in isolation.

Results

Mechanical Coupling of an Oscillatory Hair Bundle to Cyber Clones. We took advantage of an in vitro preparation of the bullfrog's saccule in which hair cells routinely display spontaneous oscillations of their hair bundles (14). In the absence of the otolithic membrane, individual hair bundles move independently from one another (22). By interfacing dynamic force clamp of a hair bundle with real-time stochastic simulations of active hair-bundle motility, we circumvented the experimental difficulty of connecting oscillatory hair bundles with actual mechanical linkages. First, we characterized the spontaneous behavior of a single hair bundle as well as its responsiveness to sinusoidal stimuli (see *Materials and Methods*). Using a physical description of active hair-bundle motility (15, 18), we adjusted parameters to quantitatively reproduce these characteristics. We thereby produced a "cyber clone" of the experimentally observed hair bundle on a computer (Fig. S1). Second, we mimicked a situation in which the hair bundle is coupled by identical springs of stiffness K to two flanking neighbors of similar characteristics, each emulated by an autonomous cyber clone (Fig. 1*A*). To this end, we calculated in real time the forces F_1 and F_2 that the two neighbors would exert on the hair bundle owing to their displacements relative to that of the hair bundle. At each time step, the sum of these forces $F_K = F_1 + F_2$ was applied to the hair bundle by actuating the position of a flexible glass fiber whose tip was affixed to the kinociliary bulb of the hair bundle (Fig. 1*B*). At the same time step, the reaction forces $-F_1$ and $-F_2$ were included in the simulations of the cyber clones. The hair bundle and the cyber clones thus dynamically influenced each other's behavior. By adding an external force F_{EXT} to both the hair bundle and the cyber clones, we could assay the effects of this dynamical interplay on hair-bundle responsiveness. Note that dynamic force clamp afforded a means to control the properties of the oscillators that interacted with the hair bundle and allowed the coupling strength to be varied at will.

Synchronization and Increased Coherence of Spontaneous Oscillations. In a first set of experiments, we studied how coupling affected the spontaneous behavior of the hair bundle in the absence of external forcing ($F_{\mathrm{EXT}} = 0$). Without coupling ($K = 0$), the spontaneous oscillations of the hair bundle and of its cyber clones were uncorrelated (Fig. 2*A*). Increasing K

Author contributions: J.B., K.D., B.L., F.J., and P.M. designed research, performed research, analyzed data, and wrote the paper.

The authors declare no conflict of interest.

This article is a PNAS Direct Submission.

[1]J.B. and K.D. contributed equally to this work.

[2]To whom correspondence should be addressed. E-mail: pascal.martin@curie.fr.

This article contains supporting information online at www.pnas.org/cgi/content/full/0913657107/DCSupplemental.

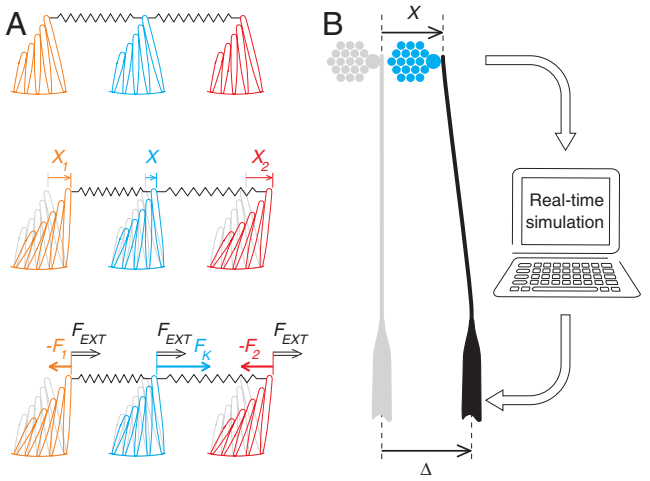

Fig. 1. Coupling a hair bundle to two cyber clones by dynamic force clamp. (*A*) Schematic representation of the coupled system. A hair bundle (blue) is connected to one neighbor on each side (orange and red) by identical springs of stiffness K. The positions of the hair bundles (X_1, X and X_2) oscillate spontaneously. Relative movements of adjacent hair bundles yield elastic forces ($-F_1$, $F_K = F_1 + F_2$ and $-F_2$). All three hair bundles experience the same external force F_{EXT}. (*B*) Experimental realization. A stimulus fiber was attached to the hair bundle's top. From each measured hair-bundle position X, the position Δ of the fiber's base was dynamically actuated to apply the force $F = F_K + F_{EXT}$ depicted in (*A*) for the central hair bundle. This force was calculated in real time from a stochastic computer simulation that emulated the behavior of the two neighbors, called cyber clones.

resulted in progressive synchronization of the oscillations, here quantified by cross-correlation coefficients (Fig. 2*B*). For $K \geq 0.4$ pN/nm, correlation coefficients exceeded 0.9, and synchronization was thus nearly complete. Notably, oscillations also became more regular with increasing coupling strengths (Fig. 2 *C*–*F*). The spectral density of both hair-bundle and cyber-clone deflections indeed sharpened (Fig. 2 *C* and *D*) and, correspondingly, it took a larger number of cycles before an oscillation lost its phase coherence. The degree of phase coherence can be described by the quality factor $Q = \nu_0/\Delta\nu$, where ν_0 is the frequency at which the spectral density of spontaneous movement peaks and $\Delta\nu$ is the width at half the maximal value. With no coupling, the hair bundle displayed a quality factor $Q = 2.2 \pm 1.0$ (mean ± SD; 33 cells). When the coupling strength K was raised from 0 to 0.4 pN/nm, we observed that Q increased until it saturated at about twice its initial value (Fig. 2*E*). A similar increase of oscillation regularity was observed with the cyber clones (Fig. 2*F*), revealing a synergic interaction between the three coupled oscillators. The cross-correlation coefficients and the relation $Q(K)$ were quantitatively reproduced by pure computer simulations of three coupled cyber clones.

Enhancement of Mechanical Amplification. In a second set of experiments, the hair bundle was subjected to a total force $F_K + F_{EXT}$, where $F_{EXT}(t) = F_0 \sin(2\pi\nu t)$ is an external stimulus of magnitude F_0 and frequency ν; the same time-dependent force F_{EXT} was included in the simulations of both cyber clones. The sensitivity of a hair bundle was defined as $|X_\nu/F_\nu|$, where X_ν and F_ν are the Fourier amplitudes of hair-bundle motion and force at the stimulus frequency, respectively. When $\nu \cong \nu_0$, the sensitivity of an oscillatory hair bundle is highest for faint stimuli and displays a compressive nonlinearity for moderate to intense stimuli (10) (Fig. 3*A*). Coupling the hair bundle to its cyber clones enhanced hair-bundle sensitivity, more so for faint stimuli ($F_0 < 1$ pN). Under such conditions, the compressive nonlinearity extended over a larger range of stimulus amplitudes. By alternating measurements of hair-bundle sensitivity with and without coupling at a low force $F_0 = 0.3$ pN, we observed that the effects of coupling were reversible (Fig. 3*B*). Moreover, the sensitivity to low stimuli increased with K, showing signs of saturation for the strongest couplings that we could achieve (Fig. 3*C*). In contrast, the sensitivity to intense stimuli ($F_0 = 50$ pN) did not depend on coupling stiffness. The gain of the hair-bundle amplifier, defined as the ratio of hair-bundle sensitivities to weak and strong stimuli, thus increased with coupling. It grew from a value of 6.0 ± 0.6 (mean ± SE; $n = 14$ cells) in the absence of coupling to 11.3 ± 0.9 for strong coupling (Fig. 3*D*). Gain enhancement of similar magnitude was also observed in the experiments for each of the cyber clones (Fig. S2). All these observations were in quantitative agreement with pure computer simulations.

Effects of Blocking the Transduction Channels. Gentamicin, an aminoglycoside antibiotic that blocks transduction channels of hair cells, affords a means to switch off the amplifier of the hair bundle (Fig. 3*D*) and thus to further assay the interplay between the hair bundle and its two cyber clones. When an oscillatory hair bundle was strongly coupled to its cyber clones, gentamicin application to the hair bundle (keeping the cyber clones unchanged) resulted in a gain reduction of the hair bundle from 11.3 ± 0.9 to 1.8 ± 0.1 ($n = 3$ cells, Fig. 3*D*). This value was only slightly larger than the gain of unity for which the hair bundle provides no amplification. Weak amplification resulted here from active driving of the passive hair bundle by oscillatory cyber clones. In addition, the amplificatory gain of the cyber clones decreased from 11.1 ± 0.8 to 3.6 ± 0.2, thus to a lower value than the gain of 5.3 ± 0.4 that was measured for the uncoupled system (Fig. S2).

Extrapolation to Larger Oscillatory Modules. We used simulations to anticipate the behavior of a larger module of coupled hair bundles. The quality factor of an oscillatory cyber clone increased almost linearly with the number of cyber clones (Fig. 4*A*). To a good approximation, gain was linearly related to the quality factor of spontaneous oscillations (Fig. 4*B*) and thus also to the number of coupled oscillators. In accordance with previous theoretical results (21), a module of only 9×9 coupled cyber clones sufficed to produce an amplificatory gain of 400 or 52 dB (Fig. 4*B*) that resembles that of the mammalian cochlea (17).

Discussion

Immersing a hair bundle into a simulated environment provided experimental insight about active mechanics at a scale intermediate between those of the single cell and the intact organ. We demonstrated that mechanical coupling of hair bundles enhances sensitivity to weak stimuli and thus enlarges the range of stimulus intensities that elicit hair-bundle vibrations beyond a given threshold. Why does coupling boost the hair-bundle amplifier? The gain of individual hair bundles is limited by intrinsic fluctuations (18–20). Coupling resulted in partial synchronization of the noisy oscillators and in an increased regularity of spontaneous oscillatory movements (Fig. 2), as observed in other oscillatory systems (23, 24). By promoting effective noise reduction, the synergic interaction between coupled hair bundles enabled each hair bundle in the group to amplify with higher gains and, as the result of the smaller bandwidth of the oscillator, with sharper frequency selectivity. In our experiments, the gain saturated at a value about twice that of the uncoupled hair bundle when the coupling stiffness K approached the hair-bundle stiffness (Fig. 3). As modest as it may seem, the measured magnitude of gain enhancement is significant considering that the hair bundle was here coupled to only two virtual neighbors. This configuration ensured that the experimental outcome was not dictated by the cyber clones. Indeed, interfering with the hair-bundle amplifier with gentamicin (Fig. 3*D*) had dramatic effects on gain enhancement, which is not the case for a large number of coupled cyber clones. Although we could have coupled the hair bundle to only one cyber clone, symmetric coupling to two

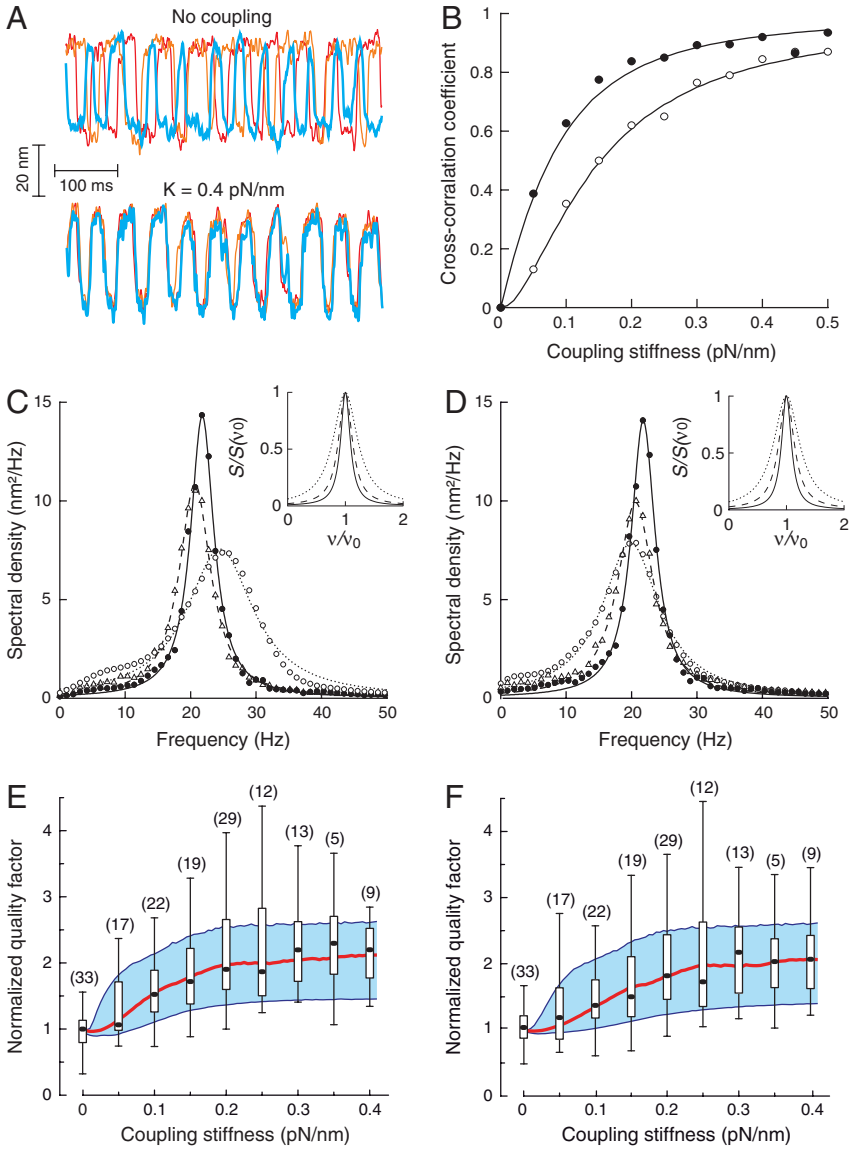

Fig. 2. Effects of coupling on spontaneous oscillations. (*A*) Spontaneous oscillations of a hair bundle (blue) and of its cyber clones (orange and red) without coupling (*Top*) and with coupling stiffness $K = 0.4$ pN/nm (*Bottom*). (*B*) Cross-correlation coefficient between the hair bundle and one cyber clone (black disks) and between the two cyber clones (white disks). Thin lines show simulation results. (*C* and *D*) Power spectral densities of hair-bundle (*C*) and one cyber-clone (*D*) movement for $K = 0$, 0.2, and 0.4 pN/nm (dotted, broken and continuous lines, respectively). The spectra were fitted by Lorentzian functions. (*Inset*) Spectra S normalized by their respective peak value $S(\nu_0)$ as a function of normalized frequencies ν/ν_0. Data in *A*–*D* from the same cell. The second cyber clone displayed a nearly identical behavior as that shown in Fig. 2*D*. (*E* and *F*) Quality factors Q of spontaneous hair-bundle (*E*) and cyber-clone (*F*) oscillations as a function of coupling stiffness K. Quality factors for any given oscillation were normalized by the mean value obtained from different measurements (typically three) of the same oscillator with no coupling. After each measurement, the quality factors of the two cyber clones of a given hair bundle were averaged. Boxes include 25% of data points above and below a median value (thick dash); whiskers delimit the total range of measured values (cell numbers at the top). Also shown are the median (red line) and the total range of values (blue area) expected for the hair bundle (*E*) or the cyber clones (*F*) from simulations for the 33 sets of parameters used in experiments. Correlation between median values obtained from experiments and simulations was quantified by a Pearson test (Fig. 2*E*: $R = 0.97$, $P < 10^{-5}$; Fig. 2*F*: $R = 0.95$, $P < 10^{-4}$).

neighbors provided stronger effects, allowed to study how the cyber clones interacted through the central hair bundle (Fig. 2*B*), and mimicked radial coupling of mammalian outer hair cells. Remarkably, all observed effects of coupling were in quantitative agreement with simulations. Our minimal description of active hair-bundle motility thus suffices to account for the effects of coupling on the hair-bundle amplifier. Reciprocally, this agreement provides strong evidence that a cyber clone can work as a realistic substitute for a hair bundle within an oscillatory module of interconnected hair bundles.

Hair bundles from the bullfrog's saccule are mechanically coupled by the overlying otolithic membrane. Given the available evidence (25, 26), we would expect strong mechanical interactions between hair bundles over the entire sensory epithelium. The saccule, however, does not show any tonotopic organization. Accordingly, frequencies of spontaneous hair-bundle oscillations, which lie within a range of 5–50 Hz, display a random spatial distribution in vitro (22). These conditions are less than ideal. Coupling-mediated enhancement is indeed facilitated if the oscillators display similar characteristics, in particular if frequency mismatches are small enough (Fig. S3). Simulations indicate that coupling heterogeneous hair-bundle oscillators can have detrimental effects on the phase coherence of spontaneous oscillations at intermediate coupling strengths. Although synchronization eventually arises when the coupling strength becomes high enough, experiments in other systems have shown that very strong coupling of nonlinear oscillators can result in a complete loss of oscillations (27). Notably, the tuning properties of individual afferent fibers innervating saccular hair cells display low quality factors ($Q < 2$) in vivo (28), similar to those of spontaneous hair-bundle oscillations in vitro and significantly lower than those evinced by electrical tuning of the hair cell's basolateral membrane (29). Unlike what would be expected in the presence of coherent spontaneous hair-bundle oscillations in vivo, there is also no evidence for multimodal histograms of interspike intervals in the spontaneous activity of saccular nerve fibers (28).

Whether the bullfrog's saccule benefits from coupling-mediated enhancement in vivo is uncertain. Nevertheless, coupling of actively oscillating hair bundles may play an important role in other systems. A ubiquitous feature of vertebrate hair cells, active hair-bundle motility has been observed in eels, frogs, turtles, chicken, and rats [reviewed in (16)]. In particular, this active process is likely to constitute a component of the cochlear amplifier in mammals (11, 30). Moreover, the various manifestations of active hair-bundle motility across species can be interpreted within the same theoretical framework (15), which suggests that properties of active hair-bundle motility observed in the frog may also apply to other species. Because auditory organs

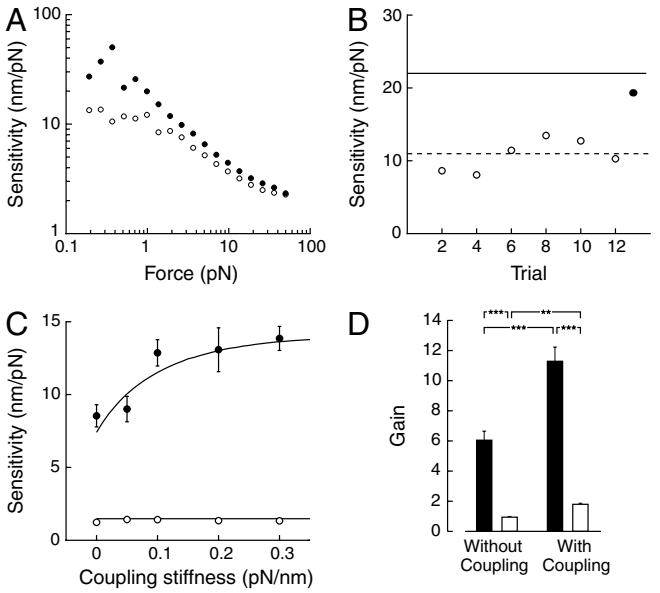

Fig. 3. Effects of coupling on nonlinear amplification. (*A*) Hair-bundle sensitivity as a function of the external force F_{EXT} without coupling (white disks) and with a coupling stiffness $K = 0.2$ pN/nm (black disks). (*B*) Hair-bundle sensitivities at $F_{EXT} = 0.3$ pN with $K = 0.2$ pN/nm (black disks) and without coupling (white disks) were significantly different (Student *t*-test $P < 5.10^{-4}$). Simulations yielded sensitivities shown by thin continuous (coupled) and dashed (uncoupled) lines that were not statistically different from mean experimental values (Student *t*-tests $P = 0.78$ and $P = 0.59$ for coupled and uncoupled conditions, respectively). (*C*) Hair-bundle sensitivity at $F_{EXT} = 0.5$ pN (black disks) and $F_{EXT} = 50$ pN (white disks) as a function of coupling stiffness. Simulations yielded similar sensitivities shown by thin lines (Pearson correlation coefficient for $F_{EXT} = 0.5$ pN: $R = 0.91$, $P = 0.03$). (*D*) Gain of the hair-bundle amplifier at saturation with $K = 0.15$–0.4 pN/nm and without coupling, under normal conditions (black) and in the presence of the channel blocker gentamicin (white). Statistical significance was estimated by a Student's *t*-test (**, $P < 0.01$; ***, $P < 0.001$).

are tonotopically organized, neighboring hair bundles display slowly varying characteristics. As suggested previously (21) and demonstrated here, a regular organization favors a synergic enhancement of hair-cells performances through mechanical coupling. This inference may be especially relevant to some bats, which devote an extended region of the cochlea—called the acoustic fovea—to echolocation near the frequency of the bat's call. In the mustached bat (*Pteronotus parnelli*), for instance, the acoustic fovea represents about 50% (7 mm) of the cochlear length (31) and thus recruits nearly half of the available hair cells (approximately 2000 outer hair cells) for the detection of a very narrow frequency band. In accordance with expectations (Fig. 4*A*), extremely sharp mechanical resonances have been measured on the basilar membrane, with quality factors $Q > 1,000$ (32). Accordingly, tuning of auditory nerve fibers in bats is much sharper than in other species. Note, however, that the bat's ability to resolve frequency modulations with uttermost precision works only for the frequency of echolocation calls.

In nonmammalian vertebrates, hair-bundle motility is the only known source of active force generation (4). In mammalian outer hair cells, active hair-bundle motility (11, 30, 33) coexists with somatic electromotility (34–36). Prestin-based electromotility has been implicated in the production of active basilar-membrane movements (37, 38). Because this process is linear over a physiological range of transmembrane potentials, the nonlinearity of the auditory amplifier is thought to emerge from mechano-electrical transduction by the hair bundle. Transduction not only provides a saturating nonlinearity that shapes the receptor potentials to which electromotility responds (6) but also electrical noise that arises from hair-bundle fluctuations. The detrimental effects of intrinsic noise on the auditory amplifier have not received much attention. Our results suggest that active hair-bundle motility can overcome this limitation (Fig. 3) and produce a compressive nonlinearity over several orders of magnitude provided that hair bundles of similar characteristics team up to form an oscillatory module at a multi cellular scale (Fig. 4). The detailed interaction between active hair-bundle motility and electromotility remains unclear. However, the nonlinearity and frequency selectivity provided by coupled hair bundles could be relayed to the basilar membrane by electromotile movements of outer hair cells within the oscillatory module. By effectively reducing noise, oscillatory modules that would each comprise a few tens of coupled hair cells could thus achieve the high gain and the sharp frequency selectivity needed by the auditory amplifier.

Materials and Methods

Experimental Preparation. Details of the experimental procedure have been published elsewhere (15). An excised preparation of the bullfrog's saccule (*Rana catesbeiana*) was mounted on a two-compartment chamber. The basal bodies of hair cells bathed in standard saline containing (in millimolar) 110 NaCl, 2 KCl, 4 $CaCl_2$, 3 D-glucose, 2 Na_2-creatine phosphate, 2 Na-pyruvate, and 5 Na-Hepes. Hair bundles instead projected in an artificial endolymph of composition (in millimolar) 2 NaCl, 118 KCl, 0.25 $CaCl_2$, 3 D-glucose, and 5 Na-Hepes. To disconnect the hair bundles from the overlying otolithic membrane, the apical surface of the preparation was exposed for 20 min to endolymph supplemented with 67 mg · ml^{-1} of the protease subtilisin

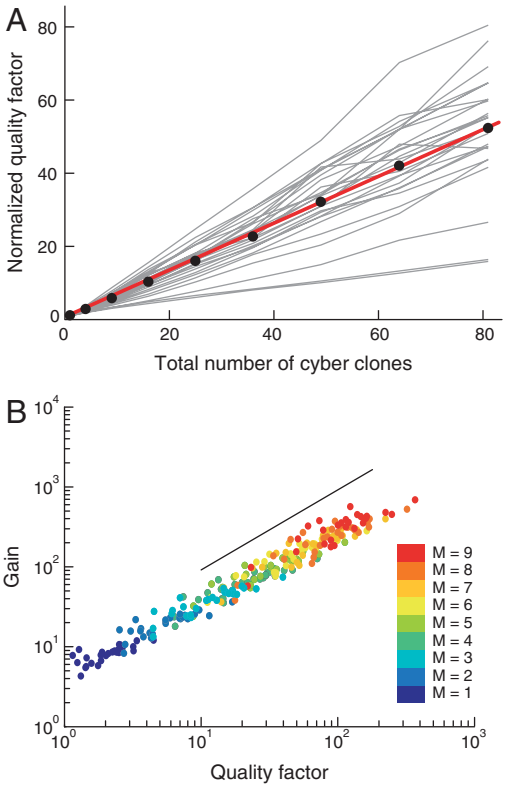

Fig. 4. Simulations of $M \times M$ identical cyber clones under strong coupling. (*A*) Quality factor Q of spontaneous cyber-clone oscillation, normalized by its value Q_1 for $M = 1$, is plotted as a function of the total number M^2 of coupled cyber clones (M is an integer between 1 and 9). Black disks correspond to average values of Q/Q_1 over the results of 27 different simulations (gray lines); each of the 27 sets of parameters defined a cyber clone of an experimentally observed hair bundle. Fit to average values (red line): $\langle Q/Q_1 \rangle = 1 + 0.64\langle M^2 - 1 \rangle$. (*B*) Amplificatory gain G of a cyber clone as a function of the quality factor Q of spontaneous oscillations for increasing sizes of the oscillatory module (color code to the right); same sets of parameters as in (*A*). A straight line of slope one is shown for comparison. Coupling strength was set at $K = 2 \times K_{SP}$, where K_{SP} represents the combined stiffness of stereociliary pivots.

(type XXIV, Sigma). The otolithic membrane was then peeled off to get access to individual hair bundles. The pH of each solution was adjusted to 7.3.

Microscopic Apparatus and Mechanical Stimulation. These methods were identical to those previously published (15). The preparation was viewed through a ×60 water-immersion objective of an upright microscope (BX51WI, Olympus). The tip of a hair bundle, or of a stimulus fiber attached to it, was imaged at a magnification of ×1, 000 onto a displacement monitor that included a dual photodiode (PIN-SPOT2D, UDT Sensor, Inc.). This photometric system was characterized by a bandwidth of 6.5 kHz at half the maximal power and yielded an output linearly proportional to the displacement of the fiber in a range of ±500 nm. Calibration was performed by measuring the output voltages of the photometric system in response to a series of offset displacements. Flexible glass fibers were fabricated from borosilicate capillaries and coated with a thin layer of gold-palladium to enhance contrast. The stiffness K_F and drag coefficient λ_F of the fibers were, respectively, 0.12–0.22 pN · nm^{-1} and 45–100 nN · s · m^{-1}, as determined by power spectral analysis of Brownian motion of the fiber's tip in water. The fiber was secured by its base to a stack type piezoelectric actuator (PA-4/12, Piezosystem Jena) driven by a custom-made power supply (Elbatech). The fiber's tip was affixed to the kinociliary bulb of an individual hair bundle. Neglecting viscous components, the force $F = K_F(\Delta - X)$ exerted by the stimulus fiber at the bundle's top was proportional to the deflection of the fiber, in which X and Δ are the positions of the hair bundle and of the fiber's base, respectively.

Characterization of an Oscillatory Hair Bundle and Creation of Cyber Clones. We characterized the properties of a hair bundle by measuring its spontaneous oscillations and its response to sinusoidal forces $F_{EXT}(t) = F_0 \sin(2\pi\nu t)$ of amplitude F_0, where t is time and ν is the stimulus frequency. The power spectral density of spontaneous hair-bundle movements displays a well-defined peak. Fitting this spectrum with a Lorentzian function (39) yields three characteristic features of the spontaneous movement: its characteristic frequency ν_0, defined as the frequency at which the spectrum peak is centered, its root-mean-squared magnitude, and its quality factor $Q = \nu_0/\Delta\nu$, where $\Delta\nu$ is the width of the spectrum at half the maximal value. The response of an oscillatory hair bundle to sinusoidal stimuli of increasing magnitudes displays a compressive nonlinearity near the characteristic frequency of oscillation (10) (Fig. 3*A*). The hair-bundle sensitivity is defined as $|X_\nu/F_\nu|$, where X_ν and F_ν are the Fourier amplitudes of hair-bundle motion and force at the stimulus frequency, respectively. In response to faint ($F_0 \cong 0.5$ pN) stimuli, the sensitivity plateaus at a maximal value. In contrast, the hair bundle displays a low sensitivity to intense ($F_0 \cong 50$ pN) stimuli. The ratio of these two quantities defines the gain of the hair-bundle amplifier.

We used a physical description of active hair-bundle motility (15, 18) to emulate quantitatively those characteristics in a computer, thereby producing "cyber clones" of the experimental hair bundle. In this description, the simulated positions X and X_a of hair bundle and adaptation motors, respectively, obeyed the following equations:

$$\lambda\dot{X} = -K_{GS}(X - X_a - DP_o) - K_{SP}X + F_{EXT}(t) + \xi(t), \qquad [1]$$

$$\lambda_a\dot{X}_a = K_{GS}(X - X_a - DP_o) - F_{max}(1 - SP_o) + \xi_a(t). \qquad [2]$$

Here, λ and λ_a are friction coefficients, K_{GS} and K_{SP} are elastic coefficients, D is the gating swing of a transduction channel, ξ_i and $\xi_{a,i}$ are Gaussian fluctuations with $\langle\xi(t)\xi(t')\rangle = 2k_BT\lambda\delta(t - t')$ and $\langle\xi_a(t)\xi_a(t')\rangle = 2k_BT_a\lambda_a\delta(t - t')$ in which $T_a = 1.5\ T$ is an effective and T the ambient temperature. $P_o = \{1 + \exp[(N\Delta G + K_{GS}D^2/2 - K_{GS}D(X - X_a))/(Nk_BT)]\}^{-1}$ is the open probability of transduction channels, where $\Delta G = 10k_BT$ is the intrinsic energy difference between open and closed states of the channels and $N = 50$ is the number of transduction elements. F_{EXT} is the external force, F_{max} is the maximal force of adaptation motors, and S quantifies calcium-mediated feedback on motors. Most parameters of the model are constrained by experimental estimates. Each parameter was thus allowed to vary only within a limited range of numerical values (Table 1).

During each experiment, a set of parameters was determined to produce stochastic simulations—here called cyber clones—that closely matched certain properties of the experimentally observed hair bundle, namely, its spectrum of spontaneous oscillations (Fig. S1) and, when necessary Fig. 3, its nonlinear response function to sinusoidal stimuli. In order to achieve a reasonable match within about 5–10 min of experimentation time, we developed two complementary strategies. First, we made use of a lookup table that listed approximately 10,000 virtual hair bundles for which we knew the quality factor, the frequency, and the root-mean-squared magnitude of spontaneous oscillations, respectively within a range of 1–5, 5–50 Hz, and 10–20 nm. This table was created by exploring a restricted region of parameter space (Table 1) and running stochastic simulations. A cyber bundle that closely matched the properties of the hair bundle could then be selected from the list and serve as cyber clone. The solution was not unique, and several sets of parameters could yield comparable results. Second, we finely tuned standard parameters that yield typical spontaneous oscillations (18) to optimize the fit between hair-bundle and cyber-clone dynamics. For this purpose, an interactive graphic interface was developed that allowed for the efficient generation and analysis of stochastic simulations within a few seconds. Applying an informed trial-and-error strategy, several parameters were varied until a close match between cyber clones and hair bundle was achieved. In particular, the frequency of cyber bundles could be adjusted at will by a uniform rescaling of the two friction coefficients λ and λ_a. The dependence of the remaining characteristics on parameter values was less accessible.

Table 1. Parameters used in stochastic simulations

Parameter	Definition	Value
λ	Friction of hair bundle	0.6–5.3 μN · s · m^{-1}
λ_a	Friction of adaptation motors	1.4–21.9 μN · s · m^{-1}
K_{GS}	Combined gating-spring stiffness	0.37–0.83 mN · m^{-1}
K_{SP}	Combined pivot stiffness	0.08–0.70 mN · m^{-1}
D	Gating-swing of a channel	51–71 nm
F_{max}	Maximal motor force	37–70 pN
S	Calcium feedback strength	0.29–1.06

All displacements and forces are expressed along the horizontal axis of a bundle's vertical plane of bilateral symmetry that contains the point of application of the external force.

Signal Generation, Acquisition. All signals were generated and acquired under the control of a master computer running a user interface programmed with LabVIEW and LabVIEW Real-Time software (version 8.5; National Instruments). The command signal controlling the external force F_{EXT} applied to the hair bundle was produced by a 16-bit interface card at a sampling rate of 2.5 kHz (PCI-6733, National Instruments). A second interface card (PCI-MIO-16E-1, National Instruments) conducted signal acquisition with a precision of 12 bit and a sampling rate of 2.5–10 kHz.

A second computer running under ETS, a real-time operating system, was equipped with a multifunction interface card (M-PCI-6259, National Instruments) for acquisition of the hair-bundle position X coming from the displacement monitor and of the force signal F_{EXT} produced by the master computer. This interface card was also used for the generation of the output signal Δ to the piezoelectric actuator that controlled the position of the stimulus fiber's base. Signals coming from the displacement monitor and going to the stimulation apparatus were conditioned with an eight-pole Bessel antialiasing filter adjusted to a low-pass half-power frequency of 1 kHz. Before each measurement, the computer received instructions from the master computer through an Ethernet port, in particular the parameters needed to produce a cyber clone of the hair bundle.

Dynamic Force Clamp. A stochastic simulation ran autonomously to mimic a situation in which a hair bundle is coupled to two neighbors of similar characteristics with elastic springs (Fig. 1). The output Δ of the simulation was function of the inputs X and F_{EXT}. At each time step $t_n = n\,dt$ (n is an integer) within a feedback loop of rate $1/dt$, here 2.5–10 kHz, the hair-bundle position $X(t_n)$ was measured. Knowing the positions $X_1(t_n)$ and $X_2(t_n)$ of two cyber clones from the previous iteration, the computer calculated the forces, $F_1 = -K \cdot (X - X_1 - X_{off})$ and $F_2 = -K \cdot (X - X_2 - X_{off})$, which originate from coupling the hair bundle to its cyber clones with an elastic spring of stiffness K (Fig. 1). To ensure that the time-averaged F_i ($i = 1, 2$) stayed close to zero, we had to compensate for slow drifts and offsets. The relative position X-X_i ($i = 1, 2$) was thus measured with respect to its mean, X_{off}, which was estimated from the last second of acquisition. The total force $F = F_1 + F_2 + F_{EXT}$ that the hair bundle should experience at t_n (with precision dt) was then applied by moving the fiber's base to position $\Delta(t_n) = F(t_n)/K_F + X(t_n)$. Knowing F_1 and F_2, the computer calculated the positions $X_1(t_{n+1})$ and $X_2(t_{n+1})$ of the two cyber clones for the next iteration by numerical integration of the dynamic equations controlling the two cyber clones:

$$\lambda \dot{X}_i = -K_{GS}(X_i - X_{a,i} - DP_{o,i}) - K_{SP}X_i - F_i(t) + F_{EXT}(t) + \xi_i(t), \quad [3]$$

$$\lambda_a \dot{X}_{a,i} = K_{GS}(X_i - X_{a,i} - DP_{o,i}) - F_{max}(1 - SP_{o,i}) + \xi_{a,i}(t). \quad [4]$$

Owing to coupling to the hair bundle, each cyber clone was subjected to a force $-F_i$ ($i = 1, 2$) that added to the external force F_{EXT}. Note that without coupling and external force ($K = 0$; $F_{EXT} = 0$), the fiber's base was required to follow the movement of its tip and was thus expected to provide no elastic load on the hair bundle. Under such circumstances, we observed that spontaneous oscillations of an uncoupled hair bundle were indeed very similar to those measured in the absence of the fiber (Fig. S4).

Simulations of $M \times M$ Coupled Cyber Clones. Details of the simulation procedure have been previously published (21). Cyber clones are arranged on a square lattice of spacing $L = 50$ μm and positioned according to their coordinates (i, j) in the xy plane, where $i = 1, \ldots, M$ and $j = 1, \ldots, M$. Cyber clones are all oriented with their excitatory direction pointing toward positive X; we denote by $X_{i,j}$ the deflection of a cyber clone along this axis and ignore perpendicular deflections. Each hair bundle is coupled by identical linear springs of stiffness K to its next nearest neighbors, including those on the two diagonal axes of the lattice. Owing to coupling, each cyber clone is subjected to a force $-F_{i,j} = \sum_{k,l} \partial U(X_{i,j}, X_{i+k,j+l})/\partial X_{i,j}$, in which the summation extends over the next nearest neighbors only and the interaction potential U is given by

$$U = \frac{K}{2}\left(\sqrt{(X_{i+k,j+l} + kL - X_{i,j})^2 + (lL)^2} - L\sqrt{k^2 + l^2}\right)^2 \quad [5]$$

We used open boundary conditions; cyber clones on the boundary thus had fewer neighbors than those in the middle of the oscillatory module.

ACKNOWLEDGMENTS. This work was supported by European Commission FP6 Integrated Project EUROHEAR, LSHG-CT-2004-512063, and by the Laboratoire Européen Associé "Active Cellular Structures" of the Centre National de la Recherche Scientifique.

1. Gold T (1948) Hearing II. The physical basis of the action of the cochlea. *Proc Roy Soc Lond B Bio* 135:492–498.
2. Dallos P (1992) The active cochlea. *J Neurosci* 12:4575–4585.
3. Hudspeth AJ (2008) Making an effort to listen: Mechanical amplification in the ear. *Neuron* 59:530–545.
4. Manley GA (2001) Evidence for an active process and a cochlear amplifier in nonmammals. *J Neurophysiol* 86:541–549.
5. Duke T, Jülicher F (2008) *Active processes and otoacoustic emissions*, eds GA Manley, AN Popper, and RR Fay (Springer, New York), pp 63–92.
6. Nobili R, Mammano F, Ashmore J (1998) How well do we understand the cochlea?. *Trends Neurosci* 21:159–167.
7. Choe Y, Magnasco MO, Hudspeth AJ (1998) A model for amplification of hair-bundle motion by cyclical binding of Ca^{2+} to mechanoelectrical-transduction channels. *Proc Natl Acad Sci USA* 95:15321–15326.
8. Camalet S, Duke T, Jülicher F, Prost J (2000) Auditory sensitivity provided by self-tuned critical oscillations of hair cells. *Proc Natl Acad Sci USA* 97:3183–3188.
9. Eguíluz VM, Ospeck M, Choe Y, Hudspeth AJ, Magnasco MO (2000) Essential nonlinearities in hearing. *Phys Rev Lett* 84:5232–5235.
10. Martin P, Hudspeth AJ (2001) Compressive nonlinearity in the hair bundle's active response to mechanical stimulation. *Proc Natl Acad Sci USA* 98:14386–14391.
11. Kennedy HJ, Crawford AC, Fettiplace R (2005) Force generation by mammalian hair bundles supports a role in cochlear amplification. *Nature* 433:880–883.
12. Crawford AC, Fettiplace R (1985) The mechanical properties of ciliary bundles of turtle cochlear hair cells. *J Physiol* 364:359–379.
13. Fettiplace R, Hackney CM (2006) The sensory and motor roles of auditory hair cells. *Nat Rev Neurosci* 7:19–29.
14. Martin P, Bozovic D, Choe Y, Hudspeth AJ (2003) Spontaneous oscillation by hair bundles of the bullfrog's sacculus. *J Neurosci* 23:4533–4548.
15. Tinevez J-Y, Jülicher F, Martin P (2007) Unifying the various incarnations of active hair-bundle motility by the vertebrate hair cell. *Biophys J* 93:4053–4067.
16. Martin P (2008) *Active processes and otoacoustic emissions*, eds GA Manley, AN Popper, and RR Fay (Springer, New York), pp 93–144.
17. Robbles L, Ruggero MA (2001) Mechanics of the mammalian cochlea. *Physiol Rev* 81:1305–1352.
18. Nadrowski B, Martin P, Jülicher F (2004) Active hair-bundle motility harnesses noise to operate near an optimum of mechanosensitivity. *Proc Natl Acad Sci USA* 101:12195–12200.
19. Jülicher F, Dierkes K, Lindner B, Prost J, Martin P (2009) Spontaneous movements and linear response of a noisy oscillator. *Eur Phys J E* 29:449–460.
20. Lindner B, Dierkes K, Jülicher F (2009) Local exponents of nonlinear compression in periodically driven noisy oscillators. *Phys Rev Lett* 103:250601.
21. Dierkes K, Lindner B, Jülicher F (2008) Enhancement of sensitivity gain and frequency tuning by coupling of active hair bundles. *Proc Natl Acad Sci USA* 105:18669–18674.
22. Ramunno-Johnson D, Strimbu CE, Fredrickson L, Arisaka K, Bozovic D (2009) Distribution of frequencies of spontaneous oscillations in hair cells of the bullfrog sacculus. *Biophys J* 96:1159–1168.
23. Chang H-C, Cao X, Mishra UK, York RA (1997) Phase noise in coupled oscillators: Theory and experiment. *IEEE T Microw Theory* 45:604–615.
24. Horikawa K, Ishimatsu K, Yoshimoto E, Kondo S, Takeda H (2006) Noise-resistant and synchronized oscillation of the segmentation clock. *Nature* 441:719–723.
25. Benser ME, Issa NP, Hudspeth AJ (1993) Hair-bundle stiffness dominates the elastic reactance to otolithic-membrane shear. *Hear Res* 68:243–252.
26. Strimbu CE, Ramunno-Johnson D, Fredrickson L, Arisaka K, Bozovic D (2009) Correlated movement of hair bundles coupled to the otolithic membrane in the bullfrog sacculus. *Hear Res* 256:58–63.
27. Ozden I, Venkataramani S, Long MA, Connors BW, Nurmikko AV (2004) Strong coupling of nonlinear electronic and biological oscillators: Reaching the "amplitude death" regime. *Phys Rev Lett* 93:158102.
28. Lewis ER (1988) Tuning in the bullfrog ear. *Biophys J* 53:441–447.
29. Hudspeth AJ, Lewis RS (1988) A model for electrical resonance and frequency tuning in saccular hair cells of the bull-frog, Rana catesbeiana. *J Physiol* 400:275–297.
30. Chan DK, Hudspeth AJ (2005) Ca^{2+} current-driven nonlinear amplification by the mammalian cochlea in vitro. *Nat Neurosci* 8:149–155.
31. Kossl M, Vater M (1985) The cochlear frequency map of the mustache bat, Pteronotus parnellii. *J Comp Physiol A* 157:687–697.
32. Kossl M, Russell IJ (1995) Basilar membrane resonance in the cochlea of the mustached bat. *Proc Natl Acad Sci USA* 92:276–279.
33. Kennedy HJ, Evans MG, Crawford AC, Fettiplace R (2006) Depolarization of cochlear outer hair cells evokes active hair bundle motion by two mechanisms. *J Neurosci* 26:2757–2766.
34. Santos-Sacchi J (2003) New tunes from Corti's organ: The outer hair cell boogie rules. *Curr Opin Neurobiol* 13:459–468.
35. Dallos P, Zheng J, Cheatham MA (2006) Prestin and the cochlear amplifier. *J Physiol* 576:37–42.
36. Ashmore J (2008) Cochlear outer hair cell motility. *Physiol Rev* 88:173–210.
37. Dallos P, et al. (2008) Prestin-based outer hair cell motility is necessary for mammalian cochlear amplification. *Neuron* 58:333–339.
38. Mellado Lagarde MM, Drexl M, Lukashkina VA, Lukashkin AN, Russell IJ (2008) Outer hair cell somatic, not hair bundle, motility is the basis of the cochlear amplifier. *Nat Neurosci* 11:746–748.
39. Martin P, Hudspeth AJ, Jülicher F (2001) Comparison of a hair bundle's spontaneous oscillations with its response to mechanical stimulation reveals the underlying active process. *Proc Natl Acad Sci USA* 98:14380–14385.

Corrections

APPLIED PHYSICAL SCIENCES, BIOPHYSICS AND COMPUTATIONAL BIOLOGY

Correction for "Coupling a sensory hair-cell bundle to cyber clones enhances nonlinear amplification," by Jérémie Barral, Kai Dierkes, Benjamin Lindner, Frank Jülicher, and Pascal Martin, which appeared in issue 18, May 4, 2010, of *Proc Natl Acad Sci USA* (107:8079–8084; first published April 19, 2010; 10.1073/pnas.0913657107).

The authors note that due to a printer's error, Fig. 3 appeared incorrectly. The corrected figure and its legend appear below.

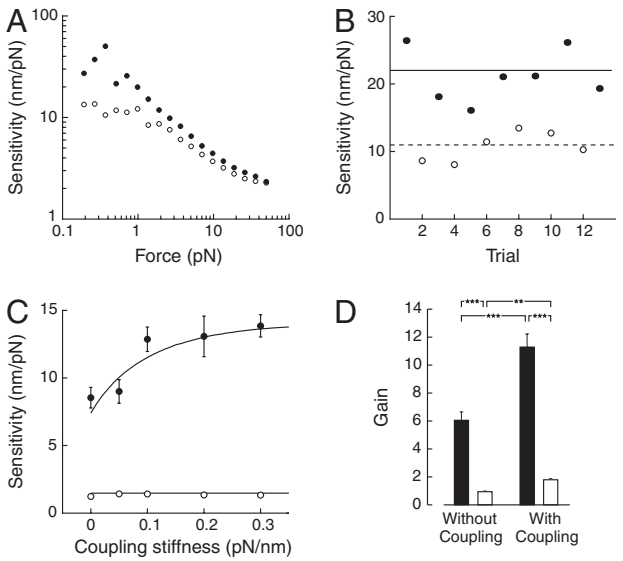

Fig. 3. Effects of coupling on nonlinear amplification. (*A*) Hair-bundle sensitivity as a function of the external force F_{EXT} without coupling (white disks) and with a coupling stiffness K = 0.2 pN/nm (black disks). (*B*) Hair-bundle sensitivities at F_{EXT} = 0.3 pN with K = 0.2 pN/nm (black disks) and without coupling (white disks) were significantly different (Student t test, $P < 5.10^{-4}$). Simulations yielded sensitivities shown by thin continuous (coupled) and dashed (uncoupled) lines that were not statistically different from mean experimental values (Student t tests, P = 0.78 and P = 0.59 for coupled and uncoupled conditions, respectively). (*C*) Hair-bundle sensitivity at F_{EXT} = 0.5 pN (black disks) and F_{EXT} = 50 pN (white disks) as a function of coupling stiffness. Simulations yielded similar sensitivities shown by thin lines (Pearson correlation coefficient for F_{EXT} = 0.5 pN: R = 0.91, P = 0.03). (*D*) Gain of the hair-bundle amplifier at saturation with K = 0.15–0.4 pN/nm and without coupling, under normal conditions (black) and in the presence of the channel blocker gentamicin (white). Statistical significance was estimated by a Student t test (**, $P < 0.01$; ***, $P < 0.001$).

www.pnas.org/cgi/doi/10.1073/pnas.1005833107

BIOCHEMISTRY

Correction for "Functional diversity among a family of human skeletal muscle myosin motors," by Daniel I. Resnicow, John C. Deacon, Hans M. Warrick, James A. Spudich, and Leslie A. Leinwand, which appeared in issue 3, January 19, 2010, of *Proc Natl Acad Sci USA* (107:1053–1058; first published December 28, 2009; 10.1073/pnas.0913527107).

The authors note the following statement should be added to the Acknowledgments: "The authors wish to correct an error in failing to explicitly acknowledge in the text the important contributions of D. Winkelmann and colleagues to the demonstration that muscle myosin requires a muscle environment to fold into a functional molecule (50–52). Their work demonstrated the expression of functional recombinant sarcomeric myosin in muscle cells. We would also like to acknowledge the technical assistance that R. Srikakulam and D. Winkelmann provided during our studies."

www.pnas.org/cgi/doi/10.1073/pnas.1005980107